

# Proton-Coupled Electron Transfer During the S-State Transitions of the Oxygen-Evolving Complex of Photosystem II

Muhammed Amin,<sup>†,||,@</sup> Leslie Vogt,<sup>‡,⊥,@</sup> Witold Szejgis,<sup>†</sup> Serguei Vassiliev,<sup>§</sup> Gary W. Brudvig,<sup>‡</sup> Doug Bruce,<sup>§</sup> and M. R. Gunner<sup>\*,†</sup>

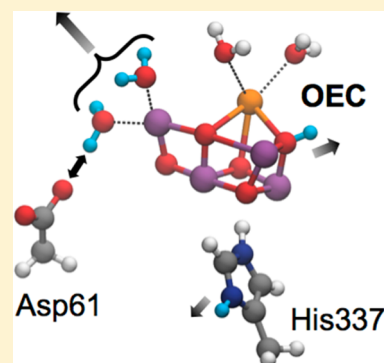
<sup>†</sup>Department of Physics, J-419, City College of New York, 138th Street, Convent Avenue, New York, New York 10031, United States

<sup>‡</sup>Department of Chemistry, Yale University, New Haven, Connecticut 06520-8107, United States

<sup>§</sup>Department of Biological Sciences, Brock University, 500 Glenridge Ave., St. Catharines, ON L2S 3A1, Canada

## Supporting Information

**ABSTRACT:** The oxygen-evolving complex (OEC) of photosystem II (PSII) is a unique  $\text{Mn}_4\text{O}_5\text{Ca}$  cluster that catalyzes water oxidation via four photoactivated electron transfer steps. As the protein influence on the redox and protonation chemistry of the OEC remains an open question, we present a classical valence model of the OEC that allows the redox state of each Mn and the protonation state of bridging  $\mu$ -oxos and terminal waters to remain in equilibrium with the PSII protein throughout the redox cycle. We find that the last bridging oxygen loses its proton during the transition from  $S_0$  to  $S_1$ . Two possible  $S_2$  states are found depending on the OEC geometry:  $S_2$  has  $\text{Mn4(IV)}$  with a proton lost from a terminal water (W1) trapped by the nearby D1-D61 if O5 is closer to Mn4, or  $\text{Mn1(IV)}$ , with partial deprotonation of D1-H337 and D1-E329 if O5 is closer to Mn1. In  $S_3$ , the OEC is  $\text{Mn}_4(\text{IV})$  with W2 deprotonated. The estimated OEC  $E_m$ 's range from +0.7 to +1.3 V, enabling oxidation by  $\text{P}_{680}^+$ , the primary electron donor in PSII. In chloride-depleted PSII, the proton release increases during the  $S_1$  to  $S_2$  transition, leaving the OEC unable to properly advance through the water-splitting cycle.



## ■ INTRODUCTION

Electron transfer reactions sit at the heart of photosynthesis. Photosystem II (PSII) harvests sunlight, initiating the process that stores solar energy in stable chemical bonds and sustains life on Earth.<sup>1–4</sup> This protein is a large ~350 kDa multisubunit complex embedded in the thylakoid membranes of green plant chloroplasts and the internal membranes of cyanobacteria.<sup>5,6</sup> The oxygen-evolving complex (OEC) within PSII accumulates the four required oxidizing equivalents at a sufficiently high potential to oxidize water to  $\text{O}_2$  at room temperature and physiological pH using the earth-abundant element Mn.<sup>2,7,8</sup> The core of the OEC is a  $\text{Mn}_4\text{O}_5\text{Ca}$  cluster bound on the lumenal side of PSII. With the advent of high-resolution structures, it has become possible to see the cluster and surrounding protein with increasing fidelity.<sup>9,10</sup> The protein contributes ligands that help control the cluster geometry, modifies the redox potential at each step, and perhaps provides a source of protons to be lost as the OEC is oxidized. However, the relative importance of the internal cluster geometry, the terminal water ligands of the OEC and the surrounding protein in controlling the thermodynamics and kinetics of the cluster has yet to be established.

Much of the understanding of how the protein environment controls electron transfer rates comes from the pioneering work of John Miller and Marshall Newton. They showed the importance of the reaction driving force and reorganization energy, as well as the role of the distance and nature of the

intervening medium in determining the reaction rates.<sup>11–14</sup> They also pioneered the analysis of electron transfer in proteins as well as smaller systems.<sup>15,16</sup> The protein environment controls the separation of the electron donor and acceptor and the nature of the intervening medium. The protein also modulates the Franck–Condon (FC) factors by tuning the free energy via modifying the long-range electrostatic potential<sup>17</sup> or by changing the direct ligands to the reactants.<sup>18</sup> The protein controls the reorganization energy by separating the reaction from water, by coupling proton and electron transfers, and through conformational changes that relax and stabilize the product states within the protein.<sup>19</sup> In photosynthetic proteins, burial of the cofactors lowers the reorganization energy, leading to faster rates at lower driving forces and reactions that can proceed rapidly and at low temperature.<sup>20</sup> Multielectron reactions are also characterized by the use of a single electron acceptor or donor.<sup>21</sup> For example the OEC is oxidized four times by a unique tyrosine,  $\text{Y}_Z$ , to oxidize water. This requires redox leveling to maintain a favorable driving force for the tyrosine to oxidize the increasingly oxidized Mn cluster, which is largely achieved through coupling the loss of electrons and protons.

**Special Issue:** John R. Miller and Marshall D. Newton Festschrift

**Received:** October 31, 2014

**Revised:** January 8, 2015

Light absorption by PSII initiates a sequence of electron transfers across the membrane, yielding a photooxidized pair of chlorophyll *a*,  $P_{680}^+$ , near the lumen and a reduced plastoquinone near the stromal side of the membrane.<sup>3,22,23</sup> The OEC reduces  $P_{680}^+$  via a redox-active tyrosine,  $Y_Z$ . In the catalytic cycle, four excitations of  $P_{680}$  will sequentially oxidize the OEC, generating five intermediate oxidation states called S states.  $S_0$  is the most reduced while  $S_4$  is the most oxidized state. On oxidation of the  $S_3$  state, the OEC extracts four electrons from two substrate water molecules to form molecular oxygen, rapidly regenerating  $S_0$ .<sup>1–4,24,25</sup>

As the OEC is oxidized, protons are lost to the lumen to keep a large positive charge from building up in the vicinity. However, it is an open question as to whether these protons come directly from bridging oxygens, substrate waters, or amino acids in the surrounding protein environment. The experimental proton release pattern, moving through the four S-state transitions ( $S_0$  to  $S_1$ ,  $S_1$  to  $S_2$ ,  $S_2$  to  $S_3$ , and  $S_3$ –[ $S_4$ ]– $S_0$ ) was initially reported as 1, 0, 1, 2.<sup>26–29</sup> More recent studies show a more realistic noninteger loss of 0.9, 0.25, 1.05, and 1.55 ( $\pm 0.1$ ),<sup>30</sup> which remains smallest in the  $S_1$  to  $S_2$  transition. An integer number of protons released indicates that the group  $pK_a$  shifts from well above the pH in one state to well below it in the subsequent state,<sup>31,32</sup> while smaller  $pK_a$  shifts lead to fractional proton loss to the lumen. Although keeping positive charge near the OEC will destabilize cluster oxidation, some buildup of positive charge near the Mn cluster through the S-state cycle is suggested by Fourier Transform Infrared (FTIR) spectroscopy.<sup>33</sup> FTIR studies suggest that a proton may move into a cluster of water near the OEC prior to release to the lumen.<sup>34,35</sup>

Studies of Mn model complexes show that the  $pK_a$  of bridging oxygens and terminal waters can shift down by as much as 10 pH units as each Mn is oxidized, making the cluster itself a likely source of the protons lost when the OEC is oxidized.<sup>31,36–39</sup> Furthermore, extended X-ray absorption fine structure (EXAFS) measurements show changes in the electronic structure and OEC geometry during the  $S_0$  to  $S_1$  and  $S_2$  to  $S_3$  transitions.<sup>40</sup> In contrast, there are no major structural changes in the transition from the  $S_1$  to the  $S_2$  state, which may help explain the lack of proton release in this transition.<sup>41,42</sup>

To investigate the source of protons released during the catalytic cycle, we must first determine the possible protonated sites of the OEC and surrounding protein residues. The  $Mn_4O_5Ca$  inorganic core of the OEC has a cubanelike structure formed by three high-valent manganese centers and a calcium connected to the fourth so-called “dangler manganese” through  $\mu$ -oxo bridges (Figure 1).<sup>9,43–52</sup> The OEC has been studied extensively using density functional theory (DFT) and quantum mechanics/molecular mechanics (QM/MM) models to explore changes in the cluster geometry and energy during the S-state cycle.<sup>53</sup> The QM/MM calculations have been tested for their ability to reproduce the available experimental EXAFS data.<sup>54–56</sup> Studies of various S states have been reported using computational models, including structures for  $S_{-1}$ ,<sup>57</sup>  $S_0$ ,<sup>56</sup>  $S_1$ ,<sup>55</sup>  $S_2$ ,<sup>58–61</sup> and more oxidized states.<sup>54,58,59,62</sup>

With four Mn centers, several oxo-bridges and terminal water ligands, it is an open question as to which center is actually oxidized in each S-state transition. The Mn cluster considered here has an oxidation state of +13 in the  $S_0$  state. Electron paramagnetic resonance (EPR) and X-ray absorption near edge spectroscopy (XANES) studies of the flash-induced S-state

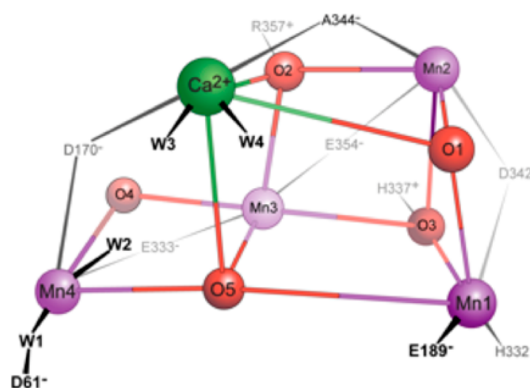


**Figure 1.** The  $Mn_4O_5Ca$  cluster and surrounding amino acids. D170 is a ligand to Mn4 and/or  $Ca^{2+}$ ; E189 and H332 are ligands to Mn1; D342 bridges Mn1 and Mn2; and E354 bridges Mn2 and Mn3. The C-terminus of A344 connects Mn2 and  $Ca^{2+}$ ; E333 connects Mn3 and Mn4. In addition, Mn4 and  $Ca^{2+}$  each have 2 water ligands. The hydrogen bonds from CP43-R357 to O2, H337 to O3, and D61 to W1 are shown. O1 and O4 make hydrogen bonds to waters in the crystal structure that are replaced with implicit solvent here. Darker lines show ligands above the plane, while gray lines are below. The Boltzmann distribution is obtained with allowed cluster microstates having each Mn (Mn1–Mn4) in the Mn(III) or Mn(IV) oxidation state, each bridging oxygen (O1–O5) in the  $OH^-$  or  $O^{2-}$  state and each water (W1–W4) as either  $H_2O$  or  $OH^-$  to be subjected to Monte Carlo sampling. Changes in charge state and position of other amino acids in the protein including those that hydrogen bond to the bridging oxygens and terminal waters are also included in the analysis.

transitions support an  $S_0$  with an oxidation state of either  $[Mn(II)Mn(III)Mn(IV)_2]$  or  $[Mn(III)_3Mn(IV)]$ ,  $S_1$  is  $[Mn(III)_2Mn(IV)_2]$  and  $S_2$  is  $[Mn(III)Mn(IV)_3]$ . Recent multi-frequency, multidimensional magnetic resonance spectroscopy shows  $S_3$  is  $[Mn(IV)_4]$ , indicating Mn-centered oxidation throughout the Kok cycle.<sup>63</sup> Other EPR measurements<sup>60</sup> as well as DFT simulations<sup>58,59</sup> also support Mn-centered oxidation, leading to  $Mn(IV)_4$  in the  $S_3$  state. There is evidence that Mn(II) is not present in the  $S_0$  state.<sup>64</sup> However, there are alternative models of an OEC that functions at a lower oxidation state, which are not considered here. In these models,  $S_0$  has an oxidation state of +11 with  $Mn(III)_3Mn(II)$  and  $O_2$  chemistry is carried out in an  $S_4$  state with a formal oxidation of  $Mn(IV)_3Mn(II)$ .<sup>65,66</sup>

A challenge for the DFT and QM/MM calculations is that they require an initial guess for the Mn oxidation states and the  $\mu$ -oxo, terminal water and amino acid protonation patterns. For example, 24 protonation states were compared for a model that includes only the direct amino acid ligands and H337 to determine the lowest energy  $S_2$  state.<sup>60</sup> The dependence of the state energy on the protonation of terminal waters and H337 has been considered.<sup>67</sup> Studies of the more reduced OEC states that are present in the X-ray structure also relied on the comparison of several, predefined protonation states.<sup>57,68</sup> DFT is also an expensive technique to treat extended regions of a protein, especially if large basis sets are used. Previous DFT studies have typically included at most the  $Mn_4O_5Ca$  cluster, terminal waters, amino acid ligands (D1–D170, D189, H332, E333, D342, A344 and CP43–E354), and amino acids that are in direct contact with the cluster through hydrogen bonding to the  $\mu$ -oxo bridges (D1–H337 and CP43–R357) in the quantum mechanical region. The rest of the protein was either treated by a dielectric continuum in DFT calculations,<sup>58,59</sup> or at the

classical molecular mechanics level in QM/MM calculations with fixed protonation states.<sup>55,56,68,69</sup>

In contrast to electronic structure methods, continuum electrostatics computations using Monte Carlo (MC) sampling can allow for the analysis of the response of the protein environment to redox reactions.<sup>70–74</sup> These MC methods have the advantage of being able to analyze the entire protein, keeping all acidic and basic residues in equilibrium with the cofactor redox changes. The difficulty with applying this approach to the OEC has been the lack of a good model for the Mn cluster that can be integrated into the classical electrostatic analysis. Recently, we developed a suitable method based on a classical valence model, including only electrostatic and Lennard-Jones interactions combined with MC sampling of possible microstates within the multiconformation continuum electrostatic (MCCE)<sup>75</sup> program. It was shown to do a remarkably good job of calculating relative  $E_m$ 's and  $pK_a$ 's of oxo-manganese clusters designed as OEC model complexes.<sup>39</sup> The advantage of this simple approach is that, in contrast with previous studies, it is not necessary to preassign the most likely distribution of redox states for the Mn and protonation states for the  $\mu$ -oxo and water ligands, as all possibilities are subjected to MC sampling.<sup>39</sup> The resulting methodology can thus address the complex problem of proton-coupled Mn oxidation reactions of the OEC of PSII, including the influence of the surrounding PSII protein residues explicitly.

The work reported here analyzes the progression of Mn oxidation states and the coupled changes in the protonation of bridging oxygens, terminal waters, and amino-acid residues in the S-state catalytic cycle. This method allows for analysis of the  $Mn_4O_5Ca$  complex more fully integrated with the rest of the protein than is possible with other computational techniques. Unlike the isolated OEC cluster model previously analyzed using electrostatics,<sup>76</sup> we see that several amino acids not typically included in previous models change protonation during the S-state transitions. Comparison of two cluster geometries using the classical electrostatic model suggests that Mn oxidation during the  $S_2/S_3$  transition may precede insertion of a new ligand between Mn1 and Mn4. Furthermore, simulations carried out with and without  $Cl^-$  indicate that  $Cl^-$  depletion may suppress  $O_2$  evolution<sup>77–79</sup> by affecting the timing of proton release from W2.

## METHODS

The 1.9 Å structure of PSII (PDB<sup>80</sup> ID 3ARC<sup>9</sup>) is used as the basis for all calculations. The MC sampling uses fixed X-ray diffraction (XRD) coordinates for the protein backbone, as well as for all cofactors other than the OEC, but side chain rotamers and protonation states are sampled for amino acids.<sup>75</sup> For each MCCE run, OEC atoms and coordinating ligands are fixed in one of two coordinate sets based on DFT optimizations reflecting  $S_1$  or  $S_3$ . The  $S_2$  state has multiple possible geometries.<sup>4,69</sup> While we do not use  $S_2$  geometries for MCCE simulations, possible  $S_2$  oxidation states and possible sources of  $S_2$  heterogeneity are discussed below. For the  $S_1$  state, we use coordinates from the QM/MM structure optimized with Mn oxidation states  $Mn_4[III,IV,IV,III]$  (the oxidation states are ordered using the numbering in Figure 1 and the 3ARC crystal structure<sup>9</sup>), all  $\mu$ -oxo bridges deprotonated and terminal waters neutral.<sup>68</sup> The OEC coordinates are taken from the QM/MM structure after alignment of the OEC ligands with the XRD coordinates.<sup>9</sup> The DFT-optimized Mn-ligand bond lengths are longer for

Mn(III) than Mn(IV). The MC sampling will reflect the DFT charge distribution due to more favorable electrostatic interactions for shorter bond lengths, favoring oxidation of Mn2 and Mn3 prior to Mn1 or Mn4 in the  $S_1$ -optimized structure.<sup>39</sup>

DFT is also used to optimize an  $S_3$  cluster model with  $Mn_4[IV,IV,IV,IV]$ , all  $\mu$ -oxo deprotonated, with W1 as  $OH^-$  and the other three terminal waters neutral. This  $Mn_4O_5Ca$  cluster is optimized using the B3LYP functional<sup>81</sup> in Gaussian09.<sup>82</sup> The LANL2DZ basis set with effective core potentials is used for Mn and Ca, while 6-31G\* is used for the other atoms.<sup>83,84</sup> Adjacent Mn centers are antiferromagnetically coupled in a  $Mn_4[\alpha,\beta,\alpha,\beta]$  scheme. The cluster DFT model includes the terminal waters bound to the dangler Mn and to  $Ca^{2+}$  (with W1 as  $OH^-$ ) and the side chains of the amino acid ligands to each Mn (D1: D170, E189, H332, E333, D342, A344 and CP43: E354). The DFT optimized geometries of both structures are reported in Figures S1 and S2 of the Supporting Information.

For the optimized  $S_3$  OEC, the position of the surrounding ligands differ from the structure found in 3ARC with a RMSD of 0.19 Å, so for this preparation, the coordinates are docked back into the PSII protein and minimized with molecular dynamics (MD) using NAMD 2.855.<sup>85</sup> Solvent is implicitly considered using the pairwise generalized Born model.<sup>86</sup> The AMBER ff99SB force field is used for all standard residues<sup>87</sup> and previously published force field parameters for PSII cofactors.<sup>87,88</sup> The distance between Mn atoms and the ligands and  $\mu$ -oxo bridges is harmonically constrained to that of the optimized DFT structure with a force constant of 20 kcal mol<sup>-1</sup> Å<sup>-2</sup>. Bending and torsion potentials between all atoms of the Mn complex are omitted. The  $Mn^{4+}$ ,  $\mu$ -oxo<sup>2-</sup>, and  $Ca^{2+}$  have formal integer charges in the MD analysis. Docking the optimized  $S_3$  OEC and ligands results in little change in the surrounding protein structure. For residues with an atom within 10 Å of the OEC, the final RMSD of the coordinates is 0.13 Å, with backbone atom positions for all but residues D1-169 to 171 in nearly the same location as for the  $S_1$  preparation (see the Supporting Information for details).

Atom-centered point charges for ligands of the OEC are determined using a method similar to that used previously for oxo-manganese model complexes.<sup>39</sup> Briefly, point charges are first determined for the full DFT model of the OEC cluster and ligands using an electrostatic potential (ESP) fit in Gaussian09.<sup>82</sup> Then an ESP fitting for just the ligands is performed with the OEC atoms replaced by point charges assigned in the first ESP run and the terminal waters given TIP charges. A more detailed description of the method and resulting ligand charges for the  $S_1$  and  $S_3$  preparation are given in Tables S1 and S2 of the Supporting Information. Our previously reported method was developed for chelating ligands that bind a single Mn center. In the OEC, several ligands bridge two metal ions, so the charges are determined for all ligands in one calculation. The net charge on the ligands is -6. Since no restraints are placed on ligand side chain charges, the net charge assigned to each anionic side chain ligand ranges from -0.97 to -1.07. The largest difference in charge assignments between the  $S_1$  and  $S_3$  OEC preparations is in the D1-H332 side chain.

For MC sampling, the intrinsic energies for isolated Mn and bridging oxygens were obtained using experimental data from model oxo-Mn complexes, as reported in our earlier work.<sup>39</sup> The solution  $pK_a$  of a bridging oxygen is determined by the experimental  $pK_a$  of the  $\mu$ -oxo in the complex  $[(bpy)_4Mn-$



(III,IV)( $\mu$ -oxo)( $\mu$ -oxoH)]<sup>4+</sup> and results in an intrinsic  $pK_a$  of the isolated bridging oxygen of 45. The experimental reduction potential of the complex [(bpy)<sub>4</sub>Mn(IV,IV)( $\mu$ -oxo)<sub>2</sub>]<sup>4+</sup> is 1.51 V vs SHE and results in a solution  $E_m$  for the gedanken Mn of 1.80 V. These previously reported values derived from the model complexes are used in this work for the OEC Mn and  $\mu$ -oxo bridges. Differences in reference values that may result from our slightly modified charge assignment method, and the subsequent effects on reported  $E_m$ 's, are discussed below.

MCCE generates an ensemble of redox and protonation states of the OEC and protonation and conformation states of the surrounding protein using standard experimental solution  $pK_a$ 's for amino acids.<sup>75</sup> The charge and position of the Mn<sub>4</sub>O<sub>5</sub>Ca cluster ligands are fixed. Chlorophylls and other PSII redox cofactors are held in their neutral form. All other amino acids throughout PSII sample appropriate protonation states, hydroxyl torsion minima, and other isosteric conformers.<sup>75</sup> In addition, amino acid residues within 15 Å of the OEC sample different side chain rotamers. MC sampling then finds the equilibrium distribution at the defined pH and  $E_h$  of the solution allowing the amino acid residues in PSII to come into equilibrium with the OEC core. (See the Supporting Information for more details on the energy terms used in MCCE sampling.) We also ran calculations for a selection of PSII residues located within 15 Å around the OEC, as is used in many QM/MM calculations, including our own.<sup>55,56,68,89</sup> While the results were qualitatively the same as for the full protein, the titratable residues on the edge of the sphere have quantitatively different protonation states. In light of this discrepancy, we use only the full protein results for our analysis. The results discussed below are for calculations at pH 6.0; changes in calculations run at pH 4 and 8 are also highlighted. Since water molecules other than terminal waters on the OEC are treated implicitly, the hydrogen-bonding network in channels around the OEC is not considered explicitly. The proximity of a water cavity on either side of D1-Y161 and D1-H190 causes the favorable MCCE conformer to have D1-H190 positively charged and the D1-Y161 OH oriented toward the space where waters would typically be located. Since a Y<sub>Z</sub> hydrogen bond interaction with D1-H190 requires a neutral imidazole, this is the only residue in the simulation for which the charged conformers are removed. In this case, MCCE selects the set of conformers in which the hydrogen atom is between Y<sub>Z</sub> and D1-H190, as expected.

To investigate the chloride dependence of the catalytic cycle, we run MCCE with fixed chloride ion occupations. Of the three chlorides reported in the 1.9 Å crystal structure, two are close to the OEC<sup>9</sup> and are investigated in more detail. Cl1 is 6.6 Å from Mn4 and 5.5 Å from D1-D61, and Cl2 is located 7.5 Å from Mn2 and 5.0 Å from D1-H337. To validate these positions, we use grand canonical Monte Carlo sampling in MCCE to determine where the chloride ions are most likely found within 10 Å of the OEC (see the Supporting Information for more details). Each of the ions with some occupancy in this simulation is within 3 Å of the 3ARC crystal structure positions<sup>9</sup> (Figure S3 of the Supporting Information). Therefore, we use crystal structure chloride locations for our simulations. Chloride-depleted runs are performed by removing each chloride independently, as well as simulating full chloride depletion.

As a check of the MCCE results, the energy of the isolated Mn<sub>4</sub>O<sub>5</sub>Ca cluster is investigated by DFT in several oxidation and protonation states identified by MC sampling. For these

calculations, the side chains (including the C<sub>β</sub> atoms) of the OEC ligands, plus D1-D61<sup>−</sup>, D1-H337<sup>+</sup>, and CP43-R357<sup>+</sup> are included in the cluster, with DFT optimization carried out as described above. In addition to the terminal water ligands of the dangler Mn and the calcium, the waters that make a hydrogen bond with  $\mu$ -oxo bridges O1 and O4 are included. All C<sub>β</sub> atoms are fixed through the geometry optimization. A total of 161 atoms are included in the DFT calculations. The geometry of the isolated clusters is optimized, given the set of defined Mn oxidation states, spin states, and bridge protonation states.

## RESULTS AND DISCUSSION

**Protein Response to OEC Oxidation.** In the MCCE simulations, the protonation states of the OEC and protein residues are kept in equilibrium with the S states as the PSII-OEC complex is oxidized. Almost all protonatable residues within 15 Å of the OEC are found to be >90% in their standard protonation states (Asp<sup>−</sup>, Glu<sup>−</sup>, His<sup>0</sup>, Lys<sup>+</sup>, and Arg<sup>+</sup>) in all S states. Furthermore, these residues change protonation by only small amounts as the OEC is oxidized, leading to at most fractional proton release to the solvent. For example, CP43-R357 remains positively charged in all S states. The only residues with protonation states coupled to OEC oxidation are D1-D61, D1-E65, D1-E329, D1-H337, D2-E312, the  $\mu$ -oxo bridge O1, and the terminal waters coordinated to Mn4 (W1 and W2). The behavior of these residues during the catalytic cycle is discussed in detail below.

**S<sub>1</sub> State of the OEC.** Parallel MCCE calculations were carried out with the OEC structure optimized in either the S<sub>1</sub> or the S<sub>3</sub> redox state. Each OEC preparation was docked into the complete PSII structure and the  $E_h$  set to ≈700 mV so that the system is in the S<sub>1</sub> oxidation state [Mn(III)<sub>2</sub>Mn(IV)<sub>2</sub>]. Unless stated otherwise, the results are similar in both structures. In the MCCE simulations, the S<sub>1</sub> state has all  $\mu$ -oxo bridges deprotonated and an oxidation state of Mn<sub>4</sub>[III,IV,IV,III]. The Mn oxidation states are in agreement with the more expensive DFT studies of the S<sub>1</sub> state,<sup>7,55,90</sup> demonstrating that the local electrostatic environment determines the relative stability of Mn(III) and Mn(IV) at each position in the cluster. The MCCE results show that in the protein environment, all terminal waters are neutral in S<sub>1</sub>. This result is in agreement with the reported QM/MM model<sup>55</sup> but disagrees with recent calculations on an isolated cluster model in a dielectric continuum, that finds that D1-H337 is neutral and the W2 ligand to Mn4 is a hydroxyl.<sup>76</sup> Our calculations, however, are at equilibrium with the full protein, indicating the importance of considering the atomistic details of the environment. The S<sub>1</sub> protonation states for the residues that change with OEC oxidation are shown in Table 1. From this starting point,  $E_h$  titrations are run to determine the behavior of the PSII protein upon OEC reduction or oxidation.

**MCCE Determination of S<sub>0</sub>.** Lowering the  $E_h$  in MCCE results in an electron being added to Mn2 along with protonation of O1 to generate S<sub>0</sub>. The local ligand charges depend on the geometry and electronic structure of the Mn<sub>4</sub>O<sub>5</sub>Ca core, which are different in the S<sub>1</sub> or S<sub>3</sub> optimized OEC cluster (Table S2 of the Supporting Information). However, both structures show Mn3 as the sole Mn(IV) center in the S<sub>0</sub> state, Mn<sub>4</sub>[III,III,IV,III]. In addition to the full protonation of the O1  $\mu$ -oxo bridge in S<sub>0</sub>, the equilibrium charge of D1-E329 also changes from partially deprotonated in S<sub>1</sub> (Table 1 and Table S5 of the Supporting Information) to be almost fully deprotonated in S<sub>0</sub>. With the cluster already in the

**Table 1. Equilibrium Charge States of Important Protein Residues in the  $S_1$  Oxidation State<sup>a</sup>**

residue	$Mn_4[III,IV,IV,III]$	
	$S_1$ preparation	$S_3$ preparation
D1-D61	−0.96	−0.99
D1-E65	−0.92	−0.95
D1-E329	−0.79	−0.49
D1-H337	+1.00	+1.00
D2-E312	−0.08	−0.05
Net local $\Delta H^+$ : $S_0$ to $S_1$	(−0.9)	(−0.6)
Net protein $\Delta H^+$ : $S_0$ to $S_1$	(−1.0)	(−0.8)

<sup>a</sup>D1-E65 and D2-E312 are close together and share one proton; the distribution of this proton is sensitive to protein preparation and  $S$  state, but there is no difference in their summed protonation. Only D1-E329 shows a significant change in the protonation state. Changes in protonation relative to the  $S_0$  state [ $Mn(III)_3Mn(IV)$ ] is also given in parentheses; local: listed residues, terminal waters, and  $\mu$ -oxo bridge O1; net protein: all residues and cofactors. One proton is lost from the  $\mu$ -oxo bridge when  $S_0$  is oxidized.

$S_1$  geometry, the  $E_m$  of the  $S_0/S_1$  transition is calculated to be −0.10 V vs SHE. A similar  $E_m$ , −0.18 V, is determined for this transition for the  $S_3$  geometry. These values are significantly more negative than the expected value of  $\approx 600$  mV estimated from the ability of  $Y_D$  ( $E_m \approx 700$  mV) to oxidize the OEC in the  $S_0$  state.<sup>91</sup> The low  $E_m$  is likely a result of several factors and suggests there may be a strong geometry dependence for the  $S_0/S_1$  transition. The position of O5 in  $S_1$  is different than in the optimized  $S_0$  form,<sup>56</sup> and the change in Mn charge also affects the ligand polarization. Thus, the OEC geometry and ligand charge assignments in MCCE strongly favor the DFT  $S_1$  or  $S_3$  redox states. In addition, while the model complexes used to parametrize the  $Mn(III)$  to  $Mn(IV)$  transition were ligands chelating one Mn,<sup>39</sup> the OEC ligands are typically bridging two Mn centers. The effect of the ligation mode on our modeling will be the focus of future work. We note, however, that calculated  $E_m$ 's for the transitions beyond  $S_1$  are reasonable and will allow the OEC to reduce  $P_{680}^+$  (see below).<sup>22,26,92,93</sup>

The MCCE result for the  $S_0$ ,  $Mn_4[III,III,IV,III]$  state with O1 protonated, differs from  $S_0$  states reported using DFT and QM/MM calculations, where the Mn oxidation is  $Mn_4[III,IV,III,III]$  with either O4 or O5 protonated.<sup>56,58</sup> Interestingly, a recent crystal structure obtained with femtosecond X-ray laser pulses in the  $S_1$  state shows bond lengths consistent with O5 being protonated.<sup>10</sup> As the MC sampling used here allows for all

possible combinations of Mn oxidation and  $\mu$ -oxo protonation, this result suggests that alternate  $S_0$  states may have been overlooked. DFT energies were compared for cluster models optimized in each of the three configurations (Mn3 oxidized with O1 protonated, and Mn2 oxidized with O4 or O5 protonated). The DFT energies of all three states are within 3.2 kcal/mol, indicating that each of these configurations may be accessible in the  $S_0$  state (Table S3 of the Supporting Information). The state with the most favorable electrostatic energy as determined by MCCE has a DFT energy between that of  $Mn_4[III,IV,III,III]$  with either O4 protonated (lowest energy) or O5 protonated (highest energy). The same energy order is found if the waters that serve as hydrogen-bonding partners for O1 and O4 are included in or removed from the DFT cluster.

Using MCCE, it is possible to evaluate states that are not selected by MC sampling, so OEC Mn redox states were explored with either O4 or O5 forced to be protonated. In either case, the favorable  $S_0$  Mn oxidation state from MCCE is  $Mn_4[III,IV,III,III]$ . If Mn2 is required to be the  $Mn(IV)$  center in the  $S_0$  state, MCCE favors protonation of O4. This proton is then lost as Mn3 is oxidized during the  $S_0/S_1$  transition. Overall, the MCCE results combined with DFT cluster analysis suggest that previously unconsidered  $S_0$  states may be possible. The classical model also supports the proton release during the  $S_0/S_1$  transition from a  $\mu$ -oxo bridge.<sup>56,58,59</sup> If the proton is constrained to be held on either O4 or O5, Mn3 oxidation to form  $S_1$  results in an extra charge on the cluster. However, there is no significant proton release from terminal waters or the surrounding protein, indicating there would be a significant buildup of charge contrary to experimental results.<sup>94</sup> This shows that even when an extra charge is constrained to remain near OEC, there are no nearby groups in the protein that have their  $pK_a$  poised so they can respond by losing a proton.

#### Limited Protein Response during the $S_1/S_2$ Transition.

While the results for the  $S_0$  and  $S_1$  states are essentially independent of the OEC geometry and ligand charges, the  $S_2$  state is more sensitive to the OEC coordinates. With the OEC cluster in the  $S_1$ -optimized geometry in which O5 is closer to Mn4, Mn4 is oxidized during the  $S_1/S_2$  transition, resulting in the oxidation state  $Mn_4[III,IV,IV,IV]$ . This transition is calculated to occur at +0.93 V and is coupled to efficient (89%) proton transfer from W1 to the neighboring D1-D61 residue (Table 2). There is also a further 7% deprotonation of W1 and 4% deprotonation of W2. A role for D61 has been

**Table 2. Equilibrium Charge States of Important Protein Residues and Terminal Waters in the  $S_2$  Oxidation State<sup>a</sup>**

residue	$Mn_4[III,IV,IV,IV]$		$Mn_4[IV,IV,IV,III]$	
	$S_1$ preparation <sup>b</sup>	$S_3$ preparation <sup>c</sup>	$S_1$ preparation <sup>b</sup>	$S_3$ preparation <sup>c</sup>
D1-D61	−0.07 (+0.89)	−0.66 (+0.33)	−0.96 (0.00)	−1.00 (−0.01)
D1-E65	−0.99 (−0.07)	−0.96 (−0.01)	−0.92 (0.00)	−1.00 (−0.05)
D1-E329	−0.96 (−0.17)	−0.80 (−0.31)	−0.92 (−0.13)	−0.98 (−0.49)
D1-H337	+1.00 (0.00)	+1.00 (0.00)	+0.15 (−0.85)	+0.85 (−0.15)
D2-E312	−0.04 (+0.04)	−0.14 (+0.09)	−0.09 (−0.01)	−0.01 (+0.04)
W1	−0.96 (−0.96)	−0.78 (−0.78)	0.00 (0.00)	0.00 (0.00)
W2	−0.04 (−0.04)	−0.02 (−0.02)	0.00 (0.00)	0.00 (0.00)
net local $\Delta H^+$ : $S_1$ to $S_2$	(−0.3)	(−0.9)	(−1.0)	(−0.7)
net protein $\Delta H^+$ : $S_1$ to $S_2$	(−0.5)	(−0.9)	(−1.0)	(−0.8)

<sup>a</sup>Changes in protonation relative to the  $S_1$  state ( $Mn_4[III,IV,IV,III]$ ) are in parentheses. <sup>b</sup>In the OEC optimized in the  $S_1$  state, oxidation of Mn4 occurs first; when the OEC is optimized in the  $S_3$  state, Mn1 oxidation is favored. <sup>c</sup>Simulations in which the Mn1 and Mn4 oxidation states were fixed rather than selected by MC sampling with a given cluster geometry.

Table 3. Equilibrium Charge States of Important Protein Residues in the  $S_3$  Oxidation State<sup>a</sup>

residue	$Mn_4[IV,IV,IV,IV]$		$Mn_4[IV,IV,IV,IV]$ with D1-H337 <sup>+</sup>	
	$S_1$ preparation	$S_3$ preparation	$S_1$ preparation	$S_3$ preparation
D1-D61	−0.28 (−0.21)	−0.65 (+0.35)	−0.58 (−0.50)	−0.99 (+0.01)
D1-E65	−0.97 (+0.02)	−0.97 (+0.03)	−0.97 (+0.02)	−0.96 (+0.01)
D1-E329	−0.96 (0.00)	−0.96 (+0.02)	−1.00 (−0.04)	−1.00 (0.00)
D1-H337	0.00 (−1.00)	+0.16 (−0.69)	+1.00 <sup>b</sup>	+1.00 <sup>b</sup>
D2-E312	−0.04 (0.00)	−0.08 (−0.07)	−0.03 (+0.01)	−0.06 (−0.02)
W1	−0.73 (+0.23)	−0.65 (−0.65)	−0.51 (+0.45)	−0.60 (−0.60)
W2	−0.41 (−0.37)	−0.30 (−0.30)	−0.90 (−0.85)	−0.40 (−0.40)
net local $\Delta H^\ddagger$ : $S_2$ to $S_3$	(−1.3)	(−1.3)	(−1.0)	(−1.0)
net protein $\Delta H^\ddagger$ : $S_2$ to $S_3$	(−1.2)	(−1.1)	(−1.0)	(−1.0)

<sup>a</sup>Changes from the  $S_2$  equilibrium protonation states are shown in parentheses. The  $S_1$  optimized OEC advances from  $Mn_4[III,IV,IV,IV]$ , and the  $S_3$  optimized structure advances from  $Mn_4[IV,IV,IV,III]$  (see Table 2). Left: D1-H337 is free to titrate. Right: D1-H337 is fixed in the protonated state, with charge differences relative to  $S_2$  with D1-H337<sup>+</sup> (see Tables S7 and S8 of the Supporting Information). <sup>b</sup>Charge fixed during simulation.

suggested from FTIR measurements<sup>95</sup> and site directed mutations.<sup>96</sup> It has also been proposed to be on the proton exit path.<sup>97,98</sup> In response to the buildup of charge near the OEC, D1-E329 shows a change in protonation state (17% deprotonation to −0.96 equilibrium charge), supporting reports that this residue is involved with the  $S_1/S_2$  transition.<sup>95</sup> The only other protein change is seen for the D1-E65 and D2-E312 pair, which loses 0.03 protons with a slight shift in which residue is protonated. These residues had been suggested to be on a proton exit path from examination of the structures,<sup>99</sup> and their sensitivity to the Kok cycle reaction is consistent with FTIR data for D1-E65 and D2-E312 mutants, indicating that this hydrogen-bonded pair is affected by the transition to  $S_2$ .<sup>95</sup> Since the MCCE calculations use implicit solvation, our results show that these residues respond to the long-range changes in electrostatic environment. Thus, this effect does not require, but does not preclude, action via local changes in an extensive hydrogen-bonding network. An  $S_2$  state composed of  $Mn_4[III,IV,IV,IV]$  with one hydroxyl ligand on  $Mn4(IV)$  is similar to the recent computational results for the  $S = 1/2$ ,  $g = 2$  multiline EPR signal,<sup>4,60</sup> although our results suggest that the deprotonated water is W1, which supports proton transfer to D61, rather than W2. Overall, 0.5–0.8 protons are calculated to be lost from PSII to the bulk upon oxidation to the  $S_2$  state (Table 2).

**Residue and OEC Water Protonation in Alternative  $S_2$  States.** Oxidation of the  $S_2$  state given the  $S_3$  optimized geometry results in both Mn1 and Mn4 titrating at almost the same  $E_m$ , with Mn1(IV) slightly lower in energy. The Mn1 oxidation in  $S_2$  has been identified with the  $g = 4.1$  EPR signal.<sup>69</sup> The  $S_3$  OEC structure in this work lacks the additional ligand that will be added in the true  $S_3$  state, but O5 is closer to Mn1 and farther from Mn4 than in the  $S_1$  optimized geometry (Figures S1 and S2 of the Supporting Information). The  $Mn_4[IV,IV,IV,III]$  state is stabilized by the position of O5 and a more negative partial charge on the ligating D1-H332 nitrogen (Table S2 of the Supporting Information) even though it lacks true octahedral coordination around Mn1.

The MCCE sampling confirms that the presence of the two  $S_2$  states is linked to changes in the location of O5 between Mn1 and Mn4 as has been suggested previously,<sup>4,69</sup> and the MCCE analysis shows that it results predominately from changes in the electrostatic interactions within the cluster. The two almost isoenergetic states are represented here by the two distinct OEC geometries used for the calculations. It is interesting to note that using the  $S_3$  optimized geometry

results in the Mn1 and Mn4 oxidations occurring at almost the same potential. As found in higher level calculations,<sup>69</sup> the classical electrostatic analysis shows the hole will be localized on the Mn center closer to O5.

In either  $S_2$  state, all bridging oxygens are deprotonated, so any proton loss during oxidation must come from other sources. Using MCCE, we can link deprotonation events in the protein to the oxidation of either Mn1 or Mn4. Independent of the OEC cluster geometry used in the calculations, Mn4 oxidation results in significant transfer of a proton from W1 to D1-D61, with some additional stabilization due to partial deprotonation of terminal waters W1 and W2 (see Table 2). If oxidation of Mn1 occurs in the presence of Mn4(III), the  $S_1/S_2$  transition is coupled to only partial deprotonation of D1-E329 and D1-H337 (discussed in more detail below). Thus, the amount and location of proton loss on forming  $S_3$  is dependent on whether the charge is lost from Mn1 or Mn4 and should thus be different in PSII showing the multiline or the  $g = 4.1$   $S_2$  EPR spectra.<sup>4,60,69</sup>

**Deprotonation during the  $S_2/S_3$  Transition.** In the MCCE calculations with the OEC  $S_1$  or  $S_3$  geometry, the  $S_2/S_3$  transition involves oxidation to the  $Mn_4[IV,IV,IV,IV]$  state. Using the  $S_1$  preparation, where the  $S_2/S_3$  transition is constrained to occur with no geometric rearrangement, the oxidation of Mn1 is calculated to be at +1.34 V, more than 500 mV higher than the  $S_1/S_2$  transition at +0.93 V. Without any geometry changes, the calculated  $E_m$  is more positive than the  $P_{680}/P_{680}^+$  redox potential of  $\sim 1.2$  V<sup>22,26,92,93</sup> but still a reasonable estimate given the error of the method ( $\sim 100$  mV).<sup>39</sup> However, when using the  $S_3$  geometry, the  $S_1/S_2$  transition with oxidation of Mn1 is calculated to be +0.70 V and the  $S_2/S_3$  transition with oxidation of Mn4 is calculated to be +0.94 V. This indicates that at least some of the redox leveling during the Kok cycle is due to rearrangement of the cluster and is not fully attributable to proton-coupled oxidation processes.

In either cluster geometry, the  $S_3$  OEC oxidation state of  $Mn_4[IV,IV,IV,IV]$  is in equilibrium with a partially deprotonated W2, partial proton transfer between D1-D61 and W1, and a mostly deprotonated D1-His337 (Table 3). After the final Mn oxidation, D1-E329 remains almost fully deprotonated, as it is in the  $S_2$  state.

**Protonation State of D1-H337.** The MCCE method results in D1-H337 deprotonation coupled to the oxidation of Mn1, regardless of whether this occurs during the transition from  $S_1$  to  $S_2$  (for the  $S_3$  preparation) or from  $S_2$  to  $S_3$  (for the



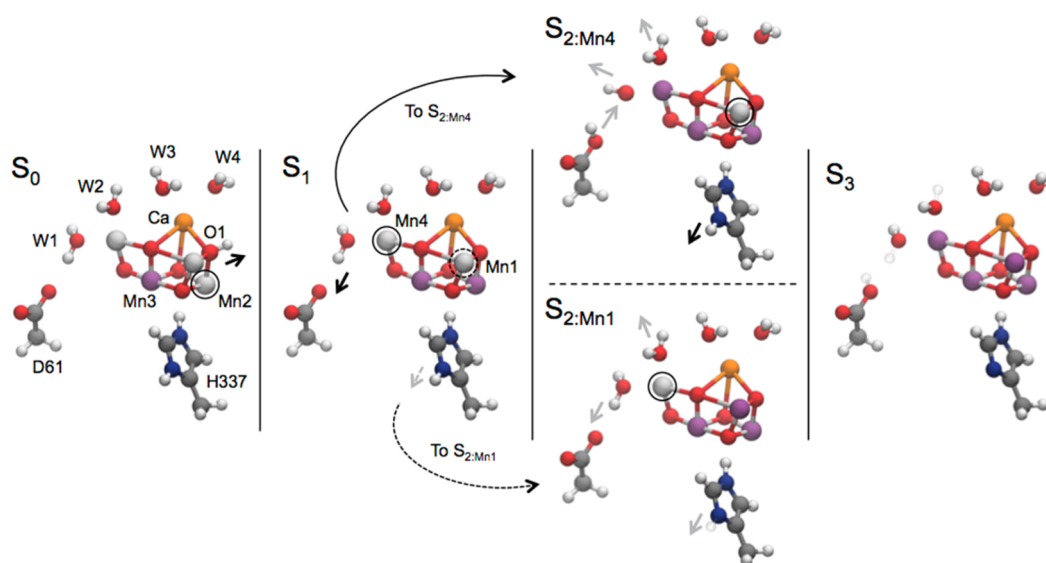


**Figure 2.** Proposed Kok cycle steps based on MCCE determined protonation patterns. The OEC atoms are shown with terminal waters W1–W4 and the side chains of D1-D61 and D1-H337. OEC atom colors indicate: Mn(III) in light gray, Mn(IV) in purple, Ca in orange. Circled Mn atoms are oxidized during the transition to the next state along with deprotonation of the indicated hydrogen atom(s). Gray arrows indicate partial deprotonation, as shown by transparent hydrogen atoms in the next S state. The  $S_1/S_2$  transition has two possibilities: via oxidation of Mn4 (solid lines to  $S_{2:Mn4}$ ) or Mn1 (dashed lines to  $S_{2:Mn1}$ ).

$S_1$  preparation). In MC calculations, redox and protonation states come to equilibrium without concern for the deprotonation pathway. The proton could be released from D1-H337 to one of two nearby water molecules that are treated implicitly in our model. However, this residue is surrounded by amino acids that cannot function as proton acceptors,<sup>100,101</sup> so losing this proton to the bulk may have a large kinetic barrier. To explore the effect of the charge remaining near the OEC, we also carried out MC sampling in which D1-H337 is constrained to remain positively charged. For both the  $S_1$  and  $S_3$  OEC geometry, the Mn oxidation order is not affected, but the extent of W1 and W2 deprotonation is changed (see Tables S7 and S8 of the Supporting Information). With D1-H337<sup>+</sup>, the proton transfer from D1-D61 back to W1 increases, with D1-D61 <42% protonated in  $S_3$  (Table 3). In addition, with a protonated His nearby, the degree of proton release from W2 increases.

**Protonation of the OEC and Protein through the S-State Cycle.** When the classical MCCE analysis is used to determine the order of Mn oxidation and proton loss from the OEC cluster, we can compare the results to detailed DFT<sup>58,59</sup> and QM/MM<sup>55,56,69</sup> calculations. The classical method provides a measure of the importance of electrostatic interactions. It also allows ready sampling of all possible states and can find low-lying redox isomers and protonation tautomers that may have been previously missed. However, the MCCE analysis is also unique in allowing us to probe how a given OEC state affects the PSII protein. This cannot be done with ab initio analysis, which typically does not include more than a few surrounding residues with preassigned protonation states. Likewise, classical MD calculations fix the protonation states in the protein region.

As the OEC is oxidized, protons are lost from PSII to the lumen. The experimental values for protons lost per OEC oxidation show less proton release upon forming  $S_2$  than the other state transitions at pH 6.<sup>26–30</sup> Overall, OEC oxidation remains coupled to proton loss from the cluster, whether from a  $\mu$ -oxo

bridge found for S states below  $S_1$  or by terminal waters in the higher oxidation states (see Figure 2). The coupling reflects the large  $pK_a$  shifts of the bridging oxygens and terminal waters upon cluster oxidation found in oxo-Mn model systems.<sup>39</sup> The MCCE calculated proton release pattern using the  $S_1$  preparation is 1.0, 0.5, 1.2 for the transitions from  $S_0$  through  $S_3$ , consistent with less proton loss during formation of  $S_2$ . Importantly, however, the proton lost from W1 upon Mn4 oxidation is mostly trapped by D1-D61 and does not reach the lumen. The proton release pattern using the  $S_3$  preparation is 0.8, 0.8, and 1.1. When Mn1 is oxidized in  $S_2$ , D1-D61 is less effective at trapping the proton (Tables 2 and 3). The region near the OEC becomes more positive in the  $S_2$  state since OEC oxidation is not fully balanced by proton loss to solution. In all simulations, a mixture of W1 and W2 deprotonation is observed, which is dependent on the OEC geometry, pH, and chloride ion concentration (see below). Both W1 and W2 are calculated to have a  $pK_a$  close to the luminal pH, which leads to W2 deprotonation being sensitive to small changes in the structure. The long-range impact of the net charge and charge distribution of the OEC affects protonation states of nearby residues, with the most significant change at D1-D61. In addition, the protonation of D1-H337 may be modulated by the S state of the OEC. The next largest contribution is from D1-E329,  $\approx 8.5$  Å from the OEC (Tables 1–3). This residue remains between 2 and 51% protonated during the catalytic cycle and is, therefore, poised to bind or release protons as the positive charge is built up near the OEC.

**Calculated  $E_m$ 's for OEC Mn Centers.** Using the Mn oxidation parameters determined from model complexes,<sup>39</sup> we have estimated the  $E_m$  of each OEC transition using the electrostatic model to within  $\pm 0.10$  V. For the  $S_1$  optimized cluster, the  $S_1/S_2$  transition is at +0.93 V, with the  $S_2/S_3$  transition occurring at +1.34 V. However, using the  $S_3$  geometry results in values of +0.70 V and +0.94 V for these transitions, with a switch in the Mn center oxidized first and much less separation between the two states. These values do not reflect

the insertion of an additional ligand in  $S_3$  but do show that the redox-leveling capacity of the OEC is assisted by geometric rearrangement and by fractional loss of protons from terminal waters. Even with the uncertainty of the benchmark calculations, the derived values are within the range required to oxidize  $P_{680}^+$ .<sup>22,26,92,93</sup> This indicates that the Mn complexes used to benchmark the MCCE calculations provide a reasonable match to the interactions occurring in the OEC within PSII.

**pH Dependence of the S-State Cycle.** The protonation states of the OEC and PSII were also determined at pH 4 and 8 (Tables S9–S14 of the Supporting Information). Altering the pH does not change the identity of the main proton acceptors corresponding to each S state; however, the degree of protonation for residues listed in Tables 1–3 decreases as the pH increases, as expected. In general, the change in protonation states of residues close to the OEC cluster due to changing pH is small, with a much greater response in other regions of the protein. However, D1-D61 and D1-E329 show changes in  $S_1$  and D1-D61, D1-E329, and D1-H337 in  $S_2$  and  $S_3$ . The relative deprotonation of terminal waters W1 and W2 is also dependent on pH. For example, in the  $S_3$  state using the  $S_1$  OEC geometry, the charge on W1 (W2) differs by +0.42 (−0.79) between pH 4 and 8. A similar variation is seen using the  $S_3$  optimized geometry (see the Supporting Information for details). The protonation state of protein residues that respond most to changes in oxidation state (D1-D61, D1-E329, and D1-H337) are also highly dependent on the pH and OEC geometry, indicating that the  $pK_a$ 's of these moieties are close to the operating pH of the PSII protein.

**Effect of Chloride.** Experimental evidence shows that the OEC cannot advance to the  $S_3$  state in the absence of chloride.<sup>77–79</sup> MC sampling is used to determine which residues are most affected by chloride removal in the  $S_2$  state. Of the three chloride ions present in the 1.9 Å crystal structure, two are located within 10 Å of the OEC.<sup>9</sup> The standard MCCE redox titration with a  $Cl^-$  solution chemical potential of  $\approx 100$  mM<sup>102</sup> results in both the chloride near D1-D61 and D2-K317 (Cl1) and the ion in the pocket near Mn2 (Cl2) remaining bound to PSII. To determine which chloride has the largest effect on the OEC oxidation states, we remove each chloride from the model separately, and also run simulations with full chloride depletion. Remarkably, removal of Cl1 does not affect the oxidation of Mn4, the closest OEC atom. Instead, the protein responds to the changed electrostatic environment by destabilizing the W1 to D1-D61 proton transfer with almost full W2 deprotonation during the  $S_1/S_2$  transition rather than on formation of  $S_3$  (Table 4). (Protonation states of important residues in chloride depleted runs are reported in Tables S15–S20 of the Supporting Information for all S states in both OEC geometries.) The removal of Cl2 results in the neutral form of D1-H337 being more favored in the  $S_2$  state, with a shift in the calculated  $E_m$  of the  $S_1/S_2$  transition of a modest <50 mV.

Together, these results show that Cl1 is primarily responsible for the need for chloride to advance in the Kok cycle, consistent with recently reported results on chloride dependence of D2-K317 mutants in this pocket<sup>103</sup> and MD simulations showing that the absence of Cl1 affects the D1-D61/D2-K317 interaction.<sup>97</sup> The additional deprotonation of W2 when chloride is not present results in a calculated proton release pattern of 1.1, 1.1, and 1.0 for the transitions from  $S_0$  through  $S_3$  for the  $S_1$  OEC geometry and 1.0, 1.0, and 0.9 for the  $S_3$  geometry. The increased proton release during the  $S_1/S_2$

**Table 4. Equilibrium Charge States of Important Protein Residues and Terminal Waters in the  $S_2$  Oxidation State  $Mn_4[III,IV,IV,IV]$  for the  $S_1$  Preparation<sup>a</sup>**

residue	$Mn_4[III,IV,IV,IV]$			
	all Cl	no Cl1	no Cl2	no Cl
D1-D61	−0.07	−0.87	−0.38	−0.85
D1-E65	−0.99	−0.96	−0.97	−0.95
D1-E329	−0.96	−0.96	−0.97	−0.95
D1-H337 <sup>b</sup>	+1.00	+1.00	+0.55	+0.37
D2-E312	−0.14	−0.09	−0.06	−0.12
W1	−0.78	−0.22	−0.89	−0.38
W2	−0.02	−0.92	−0.13	−0.92
net local $\Delta H^+$ : $S_1$ to $S_2$	(−0.3)	(−1.0)	(−0.9)	(−1.6)
net protein $\Delta H^+$ : $S_1$ to $S_2$	(−0.5)	(−1.1)	(−0.8)	(−1.1)

<sup>a</sup>Cl1: near D1-D61 and D2-K317; Cl2: near Mn2. Charge differences due to proton release from the corresponding  $S_1$  state are shown in parentheses for each case. <sup>b</sup>Charge fixed during simulation.

transition may be experimentally observable and provide additional insight into the chloride-dependence of PSII.

## CONCLUSIONS

The results reported here represent the first analysis of the OEC that is able to keep the protonation states of the cluster and full protein in equilibrium through the S-state cycle. We use a novel technique for analysis of Mn clusters developed with oxo-manganese clusters that are models of the OEC.<sup>39</sup> The advantage is that the proton affinity of the bridging oxygens and terminal waters is directly compared with that of the protein amino acids, and the Mn  $E_m$ 's are obtained with reference to the standard hydrogen electrode. These Monte Carlo calculations rely on optimizing the electrostatic energy of the system and show remarkable agreement with DFT and QM/MM assignments of the protonation and oxidation sites for the OEC in the  $S_1$ ,  $S_2$ , and  $S_3$  states. In the  $S_0$  state, the classical method finds the oxidation state  $Mn_4[III,III,IV,III]$  with O1 protonated has the lowest energy, while DFT<sup>58</sup> and QM/MM<sup>56</sup> calculations find it is  $Mn_4[III,IV,III,III]$  with O4 or O5 protonated. However, further DFT analysis shows that the  $S_0$  state of the isolated cluster has several low-lying oxidation and protonation states, including the new one suggested by the MCCE analysis.

The  $E_m$ 's calculated here for the S states up to  $S_3$  are remarkably reasonable given the simplicity of the simulation. The  $E_m$ 's for  $S_1/S_2$  and  $S_2/S_3$  are calculated to be in the range of +0.70 V to +1.34 V and show that the OEC can be oxidized once by  $P_{680}^+$  in the  $S_1$  geometry but requires a geometric change to advance past  $S_2$ . It also shows that despite the proton loss coupled to reduction, the redox leveling is not perfect. In particular, the ability of the nearby D1-D61 to trap the proton lost from Mn4 terminal water W1 prevents full proton release during the  $S_1/S_2$  transition and raises the  $E_m$  for formation of the  $S_3$  state. Subsequent oxidation to the  $Mn_4[IV,IV,IV,IV]$  state causes deprotonation of W2, the extent of which depends on local OEC structure and pH. The results also show that the protein is only modestly affected by the OEC oxidation states. Other than D1-D61, only nearby residues D1-E329, D1-H337, and the hydrogen-bonded D1-E65/D2-E312 pair show any change in protonation state throughout the cycle. This is different from the behavior of other systems such as cytochrome c oxidase<sup>104</sup> and bacterial reaction centers<sup>105–107</sup> where the distributed changes in protonation states when the



cofactors change oxidation state play a significant role in proton coupling to the redox reactions. Our results also indicate that the presence of the chloride ion near D1-D61 and D2-K317 is necessary to keep the terminal waters on Mn4 in the appropriate protonation state to advance through the catalytic cycle.

## ■ ASSOCIATED CONTENT

### ● Supporting Information

Additional information is provided for preparation of the OEC structures and associated atom information, MCCE sampling methodology, chloride ion sampling, DFT calculations for the S<sub>0</sub> state, and protonation states for important residues from MCCE titrations from S<sub>0</sub> to S<sub>3</sub>. This material is available free of charge via the Internet at <http://pubs.acs.org>.

## ■ AUTHOR INFORMATION

### Corresponding Author

\*E-mail: [gunner@sci.ccny.cuny.edu](mailto:gunner@sci.ccny.cuny.edu).

### Present Addresses

<sup>||</sup>Physical Biosciences Dept., Lawrence Berkeley National Laboratory, BLDG 64R0243 1 Cyclotron Rd, Berkeley, CA 94720.

<sup>†</sup>Department of Chemistry, New York University, New York, NY 10003.

### Author Contributions

@M.A. and L.V. contributed equally.

### Notes

The authors declare no competing financial interest.

## ■ ACKNOWLEDGMENTS

We would like to thank Victor S. Batista, Ivan Rivalta, Mehmed Z. Ertem, Sahr Khan, and David Vinyard for helpful discussions and contributions to the manuscript. We acknowledge financial support from the Division of Chemical Sciences, Geosciences, and Biosciences, Office of Basic Energy Sciences, U.S. Department of Energy (DE-SC0001423). M.R.G. also acknowledges infrastructure support from the National Center for Research Resources (Grant 2G12RR03060) and the National Institute on Minority Health and Health Disparities (Grant 8G12MD007603) from the National Institutes of Health. Biochemical work was supported by the Department of Energy, Office of Basic Energy Sciences, Division of Chemical Sciences (Grant DEFG02-05ER15646 to G.W.B.).

## ■ REFERENCES

- (1) McEvoy, J. P.; Brudvig, G. W. Water-Splitting Chemistry of Photosystem II. *Chem. Rev.* **2006**, *106* (11), 4455–4483.
- (2) Brudvig, G. W. Water Oxidation Chemistry of Photosystem II. *Philos. Trans. R. Soc. London, Ser. B* **2008**, *363* (1494), 1211–1219.
- (3) Dau, H.; Zaharieva, I. Principles, Efficiency, and Blueprint Character of Solar-Energy Conversion in Photosynthetic Water Oxidation. *Acc. Chem. Res.* **2009**, *42* (12), 1861–1870.
- (4) Cox, N.; Pantazis, D. A.; Neese, F.; Lubitz, W. Biological Water Oxidation. *Acc. Chem. Res.* **2013**, *46* (7), 1588–1596.
- (5) Diner, B. A.; Babcock, G. T. Structure, Dynamics and Energy Conservation Efficiency in Photosystem II. In *Oxygenic Photosynthesis: The Light Reactions*, Ort, D. R., Yocum, C. F., Eds.; Kluwer Academic Publishers: Dordrecht, 1996.
- (6) Barber, J.; Kuhlbrandt, W. Photosystem II. *Curr. Opin. Struct. Biol.* **1999**, *9*, 469–475.

- (7) Siegbahn, P. E. M. Water Oxidation in Photosystem II: Oxygen Release, Proton Release and the Effect of Chloride. *Dalton Trans.* **2009**, *45*, 10063–10068.
- (8) Muh, F.; Zouni, A. Light-Induced Water Oxidation in Photosystem II. *Front. Biosci.* **2011**, *17*, 3072–3132.
- (9) Umena, Y.; Kawakami, K.; Shen, J.-R.; Kamiya, N. Crystal Structure of Oxygen-Evolving Photosystem II at 1.9 Å Resolution. *Nature* **2011**, *473* (7345), 55–60.
- (10) Suga, M.; Akita, F.; Hirata, K.; Ueno, G.; Murakami, H.; Nakajima, Y.; Shimizu, T.; Yamashita, K.; Yamamoto, M.; Ago, H. Native Structure of Photosystem II at 1.95 Å Resolution Viewed by Femtosecond X-ray Pulses. *Nature* **2015**, *517*, 99–103.
- (11) Closs, G. L.; Calcaterra, L. T.; Green, N. J.; Penfield, K. W.; Miller, J. R. Distance, Stereoelectronic Effects, and the Marcus Inverted Region in Intramolecular Electron Transfer in Organic Radical Anions. *J. Phys. Chem.* **1986**, *90*, 3673–3683.
- (12) Closs, G. L.; Miller, J. M. Intramolecular Long-Distance Electron Transfer in Organic Molecules. *Science* **1988**, *240*, 440–447.
- (13) Cave, R. J.; Newton, M. D.; Kumar, K.; Zimmt, M. B. Theoretical Study of Solvent Effects on the Electronic Coupling Matrix Elements in Rigidly Linked Donor-Acceptor Systems. *J. Phys. Chem.* **1995**, *99*, 17501–17504.
- (14) Miller, J. R. Electron Transfer: Lower Tunnel Barriers. *Nat. Chem.* **2014**, *6* (10), 854–855.
- (15) Cheung, E.; Taylor, K.; Kornblatt, J. A.; English, A. M.; McLendon, G.; Miller, J. R. Direct Measurements of Intramolecular Electron Transfer Rates between cytochrome c and cytochrome c peroxidase: Effects of Exothermicity and Primary Sequence on Rate. *Proc. Natl. Acad. Sci. U.S.A.* **1986**, *83* (5), 1330–1333.
- (16) Marchi, M.; Gehlen, J. N.; Chandler, D.; Newton, M. Diabatic Surfaces and the Pathway for Primary Electron Transfer in a Photosynthetic Reaction Center. *J. Am. Chem. Soc.* **1993**, *115*, 4178–4190.
- (17) Gunner, M. R.; Nicholls, A.; Honig, B. Electrostatic Potentials in *Rhodospseudomonas viridis* Reaction Center: Implications for the Driving Force and Directionality of Electron Transfer. *J. Phys. Chem.* **1996**, *100*, 4277–4291.
- (18) Allen, J. P.; Artz, K.; Lin, X.; Williams, J. C. Effects of Hydrogen Bonding to a Bacteriochlorophyll-Bacteriopheophytin Dimer in Reaction Centers from *Rhodobacter sphaeroides*. *Biochemistry* **1996**, *35*, 6612–6619.
- (19) Ortega, J. M.; Mathis, P.; Williams, J. C.; Allen, J. P. Temperature Dependence of the Reorganization Energy for Charge Recombination in the Reaction Center from *Rhodobacter sphaeroides*. *Biochemistry* **1996**, *35*, 3354–3361.
- (20) Allen, J. P.; Williams, J. C. Relationship between the Oxidation Potential of the Bacteriochlorophyll Dimer and Electron Transfer in Photosynthetic Reaction Centers. *J. Bioenerg. Biomembr.* **1995**, *27*, 275–283.
- (21) Gunner, M. R.; Madeo, J.; Zhu, Z. Modification of Quinone Electrochemistry by the Proteins in the Biological Electron Transfer Chains: Examples from Photosynthetic Reaction Centers. *J. Bioenerg. Biomembr.* **2008**, *40* (5), 509–519.
- (22) Rappaport, F.; Diner, B. A. Primary Photochemistry and Energetics Leading to the Oxidation of the Mn<sub>4</sub>Ca Cluster and to the Evolution of Molecular Oxygen in Photosystem II. *Coord. Chem. Rev.* **2008**, *252*, 259–272.
- (23) Cardona, T.; Sedoud, A.; Cox, N.; Rutherford, A. W. Charge Separation in Photosystem II: A Comparative and Evolutionary Overview. *Biochim. Biophys. Acta* **2012**, *1817*, 26–43.
- (24) Kok, B.; Forbush, B.; McGloin, M. Cooperation of Charges in Photosynthetic O<sub>2</sub> Evolution-I. A Linear Four Step Mechanism. *Photochem. Photobiol.* **1970**, *11* (6), 457–475.
- (25) Joliot, P.; Kok, B. Oxygen Evolution in Photosynthesis. In *Bioenergetics of Photosynthesis*, Govindjee, Ed. Academic: New York, 1975; pp 387–412.
- (26) Brettel, K.; Schloder, E.; Witt, H. T. Nanosecond Reduction Kinetics of Photooxidized chlorophyll a-II (P<sub>680</sub>) in Single Flashes as a Probe for the Electron Pathway, H<sup>+</sup> Release and the Charge

Accumulation in the O<sub>2</sub>-Evolving Complex. *Biochim. Biophys. Acta* **1984**, 766, 403–415.

(27) Rappaport, F.; Lavergne, J. Proton Release During Successive Oxidation Steps of the Photosynthetic Water Oxidation Process: Stoichiometries and pH Dependence. *Biochemistry* **1991**, 30 (41), 10004–10012.

(28) Jahns, P.; Junge, W. Proton Release During the Four Steps of Photosynthetic Water Oxidation: Induction of 1:1:1:1 Pattern due to Lack of chlorophyll a/b Binding Proteins. *Biochemistry* **1992**, 31 (32), 7398–7403.

(29) Lavergne, J.; Junge, W. Proton Release During the Redox Cycle of the Water Oxidase. *Photosynth. Res.* **1993**, 38, 279–296.

(30) Suzuki, H.; Sugiura, M.; Noguchi, T. Monitoring Proton Release During Photosynthetic Water Oxidation in Photosystem II by Means of Isotope-Edited Infrared Spectroscopy. *J. Am. Chem. Soc.* **2009**, 131 (22), 7849–7857.

(31) Gunner, M. R.; Amin, M.; Zhu, X.; Lu, J. Molecular Mechanisms for Generating Transmembrane Proton Gradients. *Biochim. Biophys. Acta* **2013**, 1827 (8–9), 892–913.

(32) Lu, J.; Gunner, M. R. Characterizing the Proton Loading Site in cytochrome c oxidase. *Proc. Natl. Acad. Sci. U.S.A.* **2014**, 111, 12414–12419.

(33) Debus, R. J. FTIR Studies of Metal Ligands, Networks of Hydrogen Bonds, and Water Molecules Near the Active Site MnCaO Cluster in Photosystem II. *Biochim. Biophys. Acta* **2014**, 1847, 19–34.

(34) Noguchi, T.; Sugiura, M. FTIR Detection of Water Reactions During the Flash-Induced S-State Cycle of the Photosynthetic Water-Oxidizing Complex. *Biochemistry* **2002**, 41 (52), 15706–15712.

(35) Polander, B. C.; Barry, B. A. A Hydrogen-Bonding Network Plays a Catalytic Role in Photosynthetic Oxygen Evolution. *Proc. Natl. Acad. Sci. U.S.A.* **2012**, 109 (16), 6112–6117.

(36) Thorp, H. H.; Sarneski, J. E.; Brudvig, G. W.; Crabtree, R. H. Proton-Coupled Electron Transfer in [(bpy)<sub>2</sub>Mn(μ-O)<sub>2</sub>Mn(bpy)<sub>2</sub>]<sup>3+</sup>. *J. Am. Chem. Soc.* **1989**, 111, 9249–9250.

(37) Baldwin, M. J.; Gelasco, A.; Pecoraro, V. L. The Effect of Protonation on [Mn(IV)(μ-O)]<sub>2</sub> Complexes. *Photosynth. Res.* **1993**, 38, 303–308.

(38) Baldwin, M. J.; Pecoraro, V. L. Energetics of Proton-Coupled Electron Transfer in High-Valent Mn<sub>2</sub>(μ-O)<sub>2</sub> Systems: Models for Water Oxidation by the Oxygen-Evolving Complex of Photosystem II. *J. Am. Chem. Soc.* **1996**, 118 (45), 11325–11326.

(39) Amin, M.; Vogt, L.; Vassiliev, S.; Rivalta, I.; Sultan, M. M.; Bruce, D.; Brudvig, G. W.; Batista, V. S.; Gunner, M. R. Electrostatic Effects on Proton Coupled Electron Transfer in Oxomanganese Complexes Inspired by the Oxygen-Evolving Complex of Photosystem II. *J. Phys. Chem. B* **2013**, 117 (20), 6217–6226.

(40) Haumann, M.; Mueller, C.; Liebisch, P.; Iuzzolino, L.; Dittmer, J.; Grabolle, M.; Neisius, T.; Meyer-Klaucke, W.; Dau, H. Structural and Oxidation State Changes of the Photosystem II Manganese Complex in Four Transitions of the Water Oxidation Cycle (S<sub>0</sub> → S<sub>1</sub>, S<sub>1</sub> → S<sub>2</sub>, S<sub>2</sub> → S<sub>3</sub>, and S<sub>3,4</sub> → S<sub>0</sub>) Characterized by X-ray Absorption Spectroscopy at 20 K and Room Temperature. *Biochemistry* **2005**, 44 (6), 1894–1908.

(41) Glockner, C.; Kern, J.; Broser, M.; Zouni, A.; Yachandra, V.; Yano, J. Structural Changes of the Oxygen-Evolving Complex in Photosystem II During the Catalytic Cycle. *J. Biol. Chem.* **2013**, 288 (31), 22607–22620.

(42) Yano, J.; Yachandra, V. Mn<sub>4</sub>Ca Cluster in Photosynthesis: Where and How Water is Oxidized to Dioxygen. *Chem. Rev.* **2014**, 114 (8), 4175–4205.

(43) Hasegawa, K.; Ono, T.; Inoue, Y.; Kusunoki, M. How to Evaluate the Structure of a Tetranuclear Mn Cluster from Magnetic and EXAFS Data: Case of the S<sub>2</sub>-State Mn-Cluster in Photosystem II. *Bull. Chem. Soc. Jpn.* **1999**, 72 (5), 1013–1023.

(44) Robblee, J. H.; Messinger, J.; Cinco, R. M.; McFarlane, K. L.; Fernandez, C.; Pizarro, S. A.; Sauer, K.; Yachandra, V. K. The Mn Cluster in the S<sub>0</sub> State of the Oxygen-Evolving Complex of Photosystem II Studied by EXAFS Spectroscopy: Are There Three

di-μ-oxo-bridged Mn<sub>2</sub> Moieties in the Tetranuclear Mn Complex? *J. Am. Chem. Soc.* **2002**, 124 (25), 7459–7471.

(45) Kamiya, N.; Shen, J. Crystal Structure of Oxygen-Evolving Photosystem II from *Thermosynechococcus vulcanus* at 3.7-Ångstrom Resolution. *Proc. Natl. Acad. Sci. U.S.A.* **2003**, 100 (1), 98–103.

(46) Sauer, K.; Yachandra, V. The Water-Oxidation Complex in Photosynthesis. *Biochim. Biophys. Acta* **2004**, 1655 (1–3), 140–148.

(47) Dau, H.; Liebisch, P.; Haumann, M. The Structure of the Manganese Complex of Photosystem II in its Dark-Stable S<sub>1</sub>-State-EXAFS Results in Relation to Recent Crystallographic Data. *Phys. Chem. Chem. Phys.* **2004**, 6 (20), 4781–4792.

(48) Sauer, K.; Yano, J.; Yachandra, V. X-ray Spectroscopy of the Mn<sub>4</sub>Ca Cluster in the Water-Oxidation Complex of Photosystem II. *Photosynth. Res.* **2005**, 85 (1), 73–86.

(49) Yano, J.; Pushkar, Y.; Glatzel, P.; Lewis, A.; Sauer, K.; Messinger, J.; Bergmann, U.; Yachandra, V. High-Resolution Mn EXAFS of the Oxygen-Evolving Complex in Photosystem II: Structural Implications for the Mn<sub>4</sub>Ca Cluster. *J. Am. Chem. Soc.* **2005**, 127 (43), 14974–14975.

(50) Muh, F.; Renger, T.; Zouni, A. Crystal Structure of Cyanobacterial Photosystem II at 3.0 Å Resolution: A Closer Look at the Antenna System and the Small Membrane-Intrinsic Subunits. *Plant Physiol. Biochem.* **2008**, 46 (3), 238–264.

(51) Kawakami, K.; Umena, Y.; Kamiya, N.; Shen, J. R. Location of Chloride and its Possible Functions in Oxygen-Evolving Photosystem II Revealed by X-ray Crystallography. *Proc. Natl. Acad. Sci. U.S.A.* **2009**, 106, 8567–8572.

(52) Guskov, A.; Kern, J.; Gabdulkhakov, A.; Broser, M.; Zouni, A.; Saenger, W. Cyanobacterial Photosystem II at 2.9-Ångstrom Resolution and the Role of Quinones, Lipids, Channels and Chloride. *Nat. Struct. Mol. Biol.* **2009**, 16 (3), 334–342.

(53) Siegbahn, P. E. Water Oxidation Mechanism in Photosystem II, Including Oxidations, Proton Release Pathways, O–O Bond Formation and O<sub>2</sub> Release. *Biochim. Biophys. Acta* **2013**, 1827 (8–9), 1003–1019.

(54) Sproviero, E. M.; Gascon, J. A.; McEvoy, J. P.; Brudvig, G. W.; Batista, V. S. Quantum Mechanics/Molecular Mechanics Study of the Catalytic Cycle of Water Splitting in Photosystem II. *J. Am. Chem. Soc.* **2008**, 130 (11), 3428–3442.

(55) Lubner, S.; Rivalta, I.; Umena, Y.; Kawakami, K.; Shen, J. R.; Kamiya, N.; Brudvig, G. W.; Batista, V. S. S<sub>1</sub>-State Model of the O<sub>2</sub>-Evolving Complex of Photosystem II. *Biochemistry* **2011**, 50 (29), 6308–6311.

(56) Pal, R.; Negre, C. F.; Vogt, L.; Pokhrel, R.; Ertem, M. Z.; Brudvig, G. W.; Batista, V. S. S<sub>0</sub>-State Model of the Oxygen-Evolving Complex of Photosystem II. *Biochemistry* **2013**, 52 (44), 7703–7706.

(57) Galstyan, A.; Robertazzi, A.; Knapp, E. W. Oxygen-Evolving Mn Cluster in Photosystem II: The Protonation Pattern and Oxidation State in the High-Resolution Crystal Structure. *J. Am. Chem. Soc.* **2012**, 134 (17), 7442–7449.

(58) Siegbahn, P. E. M. An Energetic Comparison of Different Models for the Oxygen Evolving Complex of Photosystem II. *J. Am. Chem. Soc.* **2009**, 131 (51), 18238.

(59) Siegbahn, P. E. M. Structures and Energetics for O<sub>2</sub> Formation in Photosystem II. *Acc. Chem. Res.* **2009**, 42 (12), 1871–1880.

(60) Ames, W.; Pantazis, D. A.; Krewald, V.; Cox, N.; Messinger, J.; Lubitz, W.; Neese, F. Theoretical Evaluation of Structural Models of the S<sub>2</sub> State in the Oxygen Evolving Complex of Photosystem II: Protonation States and Magnetic Interactions. *J. Am. Chem. Soc.* **2011**, 133 (49), 19743–19757.

(61) Bovi, D.; Narzi, D.; Guidoni, L. The S<sub>2</sub> State of the Oxygen-Evolving Complex of Photosystem II Explored by QM/MM Dynamics: Spin Surfaces and Metastable States Suggest a Reaction Path Towards the S<sub>3</sub> State. *Angew. Chem., Int. Ed.* **2013**, 52 (45), 11744–11749.

(62) Isobe, H.; Shoji, M.; Yamanaka, S.; Umena, Y.; Kawakami, K.; Kamiya, N.; Shen, J. R.; Yamaguchi, K. Theoretical Illumination of Water-Inserted Structures of the CaMn<sub>4</sub>O<sub>5</sub> Cluster in the S<sub>2</sub> and S<sub>3</sub> States of Oxygen-Evolving Complex of Photosystem II: Full Geometry

Optimizations by B3LYP Hybrid Density Functional. *Dalton Trans.* **2012**, 41 (44), 13727–13740.

(63) Cox, N.; Retegan, M.; Neese, F.; Pantazis, D. A.; Boussac, A.; Lubitz, W. Photosynthesis. Electronic Structure of the Oxygen-Evolving Complex in Photosystem II Prior to O-O Bond Formation. *Science* **2014**, 345 (6198), 804–808.

(64) Kulik, L. V.; Epel, B.; Lubitz, W.; Messinger, J. Electronic Structure of the  $\text{Mn}_4\text{O}_x\text{Ca}$  Cluster in the  $\text{S}_0$  and  $\text{S}_2$  States of the Oxygen-Evolving Complex of Photosystem II Based on Pulse  $^{55}\text{Mn}$ -ENDOR and EPR Spectroscopy. *J. Am. Chem. Soc.* **2007**, 129 (44), 13421–13435.

(65) Kolling, D. R.; Cox, N.; Ananyev, G. M.; Pace, R. J.; Dismukes, G. C. What Are the Oxidation States of Manganese Required to Catalyze Photosynthetic Water Oxidation? *Biophys. J.* **2012**, 103 (2), 313–322.

(66) Vinyard, D. J.; Ananyev, G. M.; Dismukes, G. C. Photosystem II: The Reaction Center of Oxygenic Photosynthesis. *Annu. Rev. Biochem.* **2013**, 82, 577–606.

(67) Siegbahn, P. E. Water Oxidation Energy Diagrams for Photosystem II for Different Protonation States, and the Effect of Removing Calcium. *Phys. Chem. Chem. Phys.* **2014**, 16 (24), 11893–11900.

(68) Vogt, L.; Ertem, M. Z.; Pal, R.; Brudvig, G.; Batista, V. S. Computational Insights on Crystal Structures of the Oxygen-Evolving Complex of Photosystem II with Either  $\text{Ca}^{2+}$  or  $\text{Ca}^{2+}$  Substituted by  $\text{Sr}^{2+}$ . *Biochemistry* **2015**, DOI: 10.1021/bi5011706.

(69) Pantazis, D. A.; Ames, W.; Cox, N.; Lubitz, W.; Neese, F. Two Interconvertible Structures that Explain the Spectroscopic Properties of the Oxygen-Evolving Complex of Photosystem II in the  $\text{S}_2$  State. *Angew. Chem., Int. Ed.* **2012**, 51 (39), 9935–9940.

(70) Ullmann, G. M.; Kloppmann, E.; Essigke, T.; Krammer, E.-M.; Klingen, A. R.; Becker, T.; Bombarda, E. Investigating the Mechanisms of Photosynthetic Proteins Using Continuum Electrostatics. *Photosynth. Res.* **2008**, 97 (1), 33–53.

(71) Krishtalik, L. I. Continuum Electrostatics of Proteins: Experimental Test with Model Solvents and the Method of the Proteins pK Calculations. *J. Chem. Phys.* **2005**, 123, 316–329.

(72) Mao, J.; Hauser, K.; Gunner, M. R. How cytochromes with Different Folds Control heme Redox Potentials. *Biochemistry* **2003**, 42 (33), 9829–9840.

(73) Gunner, M. R.; Mao, J.; Song, Y.; Kim, J. Factors Influencing Energetics of Electron and Proton Transfers in Proteins. What Can be Learned from Calculations. *Biochim. Biophys. Acta* **2006**, 1757, 942–968.

(74) Ishikita, H.; Morra, G.; Knapp, E. W. Redox Potential of Quinones in Photosynthetic Reaction Centers from *Rhodospirillum rubrum*: Dependence on Protonation of Glu-L212 and Asp-L213. *Biochemistry* **2003**, 42 (13), 3882–3892.

(75) Song, Y. F.; Mao, J. J.; Gunner, M. R. MCCE2: Improving Protein pK<sub>a</sub> Calculations with Extensive Side Chain Rotamer Sampling. *J. Comput. Chem.* **2009**, 30 (14), 2231–2247.

(76) Robertazzi, A.; Galst'yan, A.; Knapp, E. W. PSII Manganese Cluster: Protonation of W2, O5, O4 and His337 in the  $\text{S}_1$  State Explored by Combined Quantum Chemical and Electrostatic Energy Computations. *Biochim. Biophys. Acta, Bioenerg.* **2014**, 1837 (8), 1316–1321.

(77) Homann, P. H. Chloride and Calcium in Photosystem II: From Effects to Enigma. *Photosynth. Res.* **2002**, 73, 169–175.

(78) Olesen, K.; Andreasson, L. E. The Function of the Chloride Ion in Photosynthetic Oxygen Evolution. *Biochemistry* **2003**, 42 (7), 2025–2035.

(79) Pokhrel, R.; McConnell, I. L.; Brudvig, G. W. Chloride Regulation of Enzyme Turnover: Application to the Role of Chloride in Photosystem II. *Biochemistry* **2011**, 50 (14), 2725–2734.

(80) Berman, H. M.; Westbrook, J.; Feng, Z.; Gilliland, G.; Bhat, T. N.; Weissig, H.; Shindyalov, I. N.; Bourne, P. E. The Protein Data Bank. *Nucleic Acids Res.* **2000**, 28, 235–242.

(81) Becke, A. D. Density-Functional Thermochemistry 0.3. The Role of Exact Exchange. *J. Chem. Phys.* **1993**, 98 (7), 5648–5652.

(82) Frisch, M. J.; Trucks, G. W.; Schlegel, H. B.; Scuseria, G. E.; Robb, M. A.; Cheeseman, J. R.; Scalmani, G.; Barone, V.; Mennucci, B.; Petersson, G. A., et al. *Gaussian 09*, revision A.1; Gaussian Inc.: Wallingford, CT, 2009.

(83) Hay, P. J.; Wadt, W. R. Ab initio Effective Core Potentials for Molecular Calculations. Potentials for the Transition Metal Atoms Sc to Hg. *J. Chem. Phys.* **1985**, 82 (1), 270–283.

(84) Petersson, G. A.; Al-Laham, M. A. A Complete Basis Set Model Chemistry. II. Open-Shell Systems and the Total Energies of the First-Row Atoms. *J. Chem. Phys.* **1991**, 94.

(85) Phillips, J. C.; Braun, R.; Wang, W.; Gumbart, J.; Tajkhorshid, E.; Villa, E.; Chipot, C.; Skeel, R. D.; Kale, L.; Schulten, K. Scalable Molecular Dynamics with NAMD. *J. Comput. Chem.* **2005**, 26 (16), 1781–1802.

(86) Still, W. C.; Tempczyk, A.; Hawley, R. C.; Hendrickson, T. Semianalytical Treatment of Solvation for Molecular Mechanics and Dynamics. *J. Am. Chem. Soc.* **1990**, 112, 6127–6129.

(87) Case, D. A.; Cheatham, T. E.; Darden, T.; Gohlke, H.; Luo, R.; Merz, K. M.; Onufriev, A.; Simmerling, C.; Wang, B.; Woods, R. J. The Amber Biomolecular Simulation Programs. *J. Comput. Chem.* **2005**, 26 (16), 1668–1688.

(88) Vasil'ev, S.; Bruce, D. A Protein Dynamics Study of Photosystem II: The Effects of Protein Conformation on Reaction Center Function. *Biophys. J.* **2006**, 90 (9), 3062–3073.

(89) Retegan, M.; Neese, F.; Pantazis, D. A. Convergence of QM/MM and Cluster Models for the Spectroscopic Properties of the Oxygen-Evolving Complex in Photosystem II. *J. Chem. Theory Comput.* **2013**, 9 (8), 3832–3842.

(90) Siegbahn, P. E. Recent Theoretical Studies of Water Oxidation in Photosystem II. *J. Photochem. Photobiol., B* **2011**, 104 (1–2), 94–99.

(91) Vass, I.; Styring, S. pH-Dependent Charge Equilibria between Tyrosine-D and the S States in Photosystem II. Estimation of Relative Midpoint Redox Potentials. *Biochemistry* **1991**, 30, 830–839.

(92) Rappaport, F.; Lavergne, J. Charge Recombination and Proton Transfer in Manganese-Depleted Photosystem II. *Biochemistry* **1997**, 36 (49), 15294–15302.

(93) Rappaport, F.; Guergova-Kuras, M.; Nixon, P. J.; Diner, B. A.; Lavergne, J. Kinetics and Pathways of Charge Recombination in Photosystem II. *Biochemistry* **2002**, 41 (26), 8518–8527.

(94) Klauss, A.; Haumann, M.; Dau, H. Alternating Electron and Proton Transfer Steps in Photosynthetic Water Oxidation. *Proc. Natl. Acad. Sci. U.S.A.* **2012**, 109 (40), 16035–16040.

(95) Service, R. J.; Hillier, W.; Debus, R. J. Evidence from FTIR Difference Spectroscopy of an Extensive Network of Hydrogen Bonds Near the Oxygen-Evolving  $\text{Mn}_4\text{Ca}$  Cluster of Photosystem II Involving D1-Glu65, D2-Glu312, and D1-Glu329. *Biochemistry* **2010**, 49 (31), 6655–6669.

(96) Dilbeck, P. L.; Hwang, H. J.; Zaharieva, I.; Gerencser, L.; Dau, H.; Burnap, R. L. The D1-D61N Mutation in *Synechocystis* sp. PCC 6803 Allows the Observation of pH-Sensitive Intermediates in the Formation and Release of  $\text{O}_2$  from Photosystem II. *Biochemistry* **2012**, 51 (6), 1079–1091.

(97) Rivalta, I.; Amin, M.; Luber, S.; Vassiliev, S.; Pokhrel, R.; Umena, Y.; Kawakami, K.; Shen, J. R.; Kamiya, N.; Bruce, D.; et al. Structural-Functional Role of Chloride in Photosystem II. *Biochemistry* **2011**, 50 (29), 6312–6315.

(98) Siegbahn, P. E. Mechanisms for Proton Release During Water Oxidation in the  $\text{S}_2$  to  $\text{S}_3$  and  $\text{S}_3$  to  $\text{S}_4$  Transitions in Photosystem II. *Phys. Chem. Chem. Phys.* **2012**, 14 (14), 4849–4856.

(99) Bondar, A. N.; Dau, H. Extended Protein/Water H-Bond Networks in Photosynthetic Water Oxidation. *Biochim. Biophys. Acta* **2012**, 1817 (8), 1177–1190.

(100) Gabdulkhakov, A.; Guskov, A.; Broser, M.; Kern, J.; Muh, F.; Saenger, W.; Zouni, A. Probing the Accessibility of the  $\text{Mn}_4\text{Ca}$  Cluster in Photosystem II: Channels Calculation, Noble Gas Derivatization, and Cocrystallization with DMSO. *Structure* **2009**, 17 (9), 1223–1234.

(101) Vassiliev, S.; Zaraiskaya, T.; Bruce, D. Molecular Dynamics Simulations Reveal Highly Permeable Oxygen Exit Channels Shared



with Water Uptake Channels in Photosystem II. *Biochim. Biophys. Acta* **2013**, 1827 (10), 1148–1155.

(102) Song, Y.; Gunner, M. R. Using Multi-Conformation Continuum Electrostatics to Compare Chloride Binding Motifs in  $\alpha$ -amylase, human serum albumin, and Omp32. *J. Mol. Biol.* **2009**, 387, 840–856.

(103) Pokhrel, R.; Service, R. J.; Debus, R. J.; Brudvig, G. W. Mutation of Lysine 317 in the D2 Subunit of Photosystem II Alters Chloride Binding and Proton Transport. *Biochemistry* **2013**, 52 (28), 4758–4773.

(104) Song, Y.; Michonova-Alexova, E.; Gunner, M. R. Calculated Proton Uptake on Anaerobic Reduction of cytochrome c oxidase: Is the Reaction Electroneutral? *Biochemistry* **2006**, 45, 7959–7975.

(105) Alexov, E.; Gunner, M. R. Calculated Protein and Proton Motions Coupled to Electron Transfer: Electron Transfer from  $Q_A^-$  to  $Q_B$  in Bacterial Photosynthetic Reaction Centers. *Biochemistry* **1999**, 38, 8254–8270.

(106) Lancaster, C. R. D.; Michel, H.; Honig, B.; Gunner, M. R. Calculated Coupling of Electron and Proton Transfer in the Photosynthetic Reaction Center of *Rhodospseudomonas viridis*. *Biophys. J.* **1996**, 70, 2469–2492.

(107) Ishikita, H.; Knapp, E. W. Variation of Ser-L223 Hydrogen Bonding with the  $Q_B$  Redox State in Reaction Centers from *Rhodobacter sphaeroides*. *J. Am. Chem. Soc.* **2004**, 126 (25), 8059–8064.